15TH IEA HEAT PUMP CONFERENCE
MAY 26–29, 2026 | HOFBURG VIENNA 2026
DECARBONISATION THROUGH INNOVATION

Development and performance evaluation of an R718 heat pump system using an electrochemical compressor

Chanho Chu[a], Minsung Kim[b], Dong Kyu Kim[a,c*]

[a]School of Mechanical Engineering, Chung-Ang university, Seoul 06974, Korea
[b]*School of Energy systems Engineering, Chung-Ang university, Seoul 06974, Korea*
[c]School of Computer science and Engineering, Chung-Ang university, Seoul 06974, Korea

Abstract

This study investigates the thermodynamic performance of an R718/hydrogen heat pump system integrating an electrochemical compressor (EC) as an alternative to conventional mechanical vapor compression, specifically targeting low-pressure and low-temperature cooling applications where conventional compressors exhibit limited efficiency. A comprehensive system-level model was developed using MATLAB and REFPROP to evaluate the effects of key operating parameters, including condenser pressure and evaporator pressure, on the coefficient of performance (COP) and cooling capacity. Increasing the condenser pressure to 60 kPa enhanced R718 condensation and maximized the COP at 4.2, beyond which the COP declined due to increased reversible electrochemical power. The evaporator pressure showed a linear positive effect on COP, reaching 4.6 at 7 kPa, primarily due to a reduced pressure ratio and lower electrochemical work. The results demonstrate the feasibility of electrochemical compression for R718-based heat pump systems and indicate its suitability for high-efficiency, low-GWP heat pump applications operating under low-pressure conditions.

Selection and/or peer-review under the responsibility of the organizers of the 15th IEA Heat Pump Conference 2026.

Keywords: Heat pump; Electrochemical compressor; R718 refrigerant; hydrogen refrigerant; Isothermal compression ;

1. Introduction

Heat pumps are widely recognized as one of the most effective technologies for achieving high energy efficiency and low carbon emissions in heating, ventilation, and air-conditioning (HVAC) systems [1]. As global regulations increasingly restrict the use of refrigerants with high global warming potential (GWP), the transition toward environmentally benign working fluids has become a critical research priority [2]. In this context, natural refrigerants have attracted significant attention due to their negligible GWP and long-term sustainability.

Among natural refrigerants, R718 (water) offers clear environmental and safety advantages, including zero global warming potential and zero ozone depletion potential. In addition, water is readily available and chemically stable, making R718 an attractive refrigerant for sustainable heat pump applications. These characteristics make R718 a promising refrigerant for sustainable heat pump applications. Nevertheless, despite these advantages, the application of R718 in conventional vapor-compression heat pump systems remains limited by intrinsic thermophysical challenges, including extremely low saturation pressure at ambient temperatures and a large specific volume ratio across the compression process [3]. These characteristics lead to high compression ratios, large compressor displacement requirements, and reduced mechanical efficiency when mechanical compressors are employed. Consequently, alternative compression concepts are required to fully exploit the environmental and safety benefits of R718-based heat pump systems.

Electrochemical compressors (ECs) have emerged as a promising non-mechanical compression technology that enables near-isothermal gas compression through electrochemical reactions, eliminating moving parts and associated mechanical losses [4]. Extensive studies have demonstrated the feasibility of ECs for hydrogen and

* Corresponding author. *E-mail address:* dkyukim@cau.ac.kr

ammonia compression, highlighting advantages in efficiency, durability, and operational stability [5]. More recently, the concept of electrochemical compression has been extended to R718-related systems by utilizing hydrogen as an electrochemical working species, indicating the potential for EC-driven R718 heat pump applications [6]. However, the majority of existing studies have focused on component-level EC performance, such as polarization behavior, compression efficiency, or pressure capability, without sufficiently addressing the interactions between electrochemical compression and the overall heat pump cycle [7].

A comprehensive system-level analysis is essential to evaluate the practical applicability of EC-integrated heat pumps, particularly for R718, where cycle performance is highly sensitive to pressure levels, phase separation behavior, and auxiliary power consumption. To date, the coupled effects of electrochemical compression, heat exchange processes, phase separation, and expansion on the overall coefficient of performance (COP) and cooling capacity have not been systematically investigated.

In this study, a fully integrated R718/hydrogen heat pump cycle model is developed, incorporating electrochemical compression, phase separation, heat exchangers, and expansion processes within a unified framework. A parametric analysis is conducted to quantify the influence of condenser pressure and evaporator pressure on system COP and EC power demand. Through this approach, the present work provides fundamental insights into the design and operating conditions required to realize high-efficiency heat pump systems employing electrochemical compression, thereby clarifying the system-level role of ECs in next-generation R718 heat pump application.

2. Methods

2.1. System configuration

Fig. 1 shows the schematic configuration of the R718 heat pump system using an EC and the corresponding pressure–enthalpy (P–h) diagram. As shown in Fig. 1(b), a mixture of liquid R718 and hydrogen gas enters the system at the inlet (state 1). Hydrogen is used as a carrier gas for electrochemical compression, while R718 serves as the refrigerant in the heat pump cycle. The mixture is supplied to the EC and isothermally compressed to a higher pressure, exiting the EC at (state 2). Inside the EC, hydrogen acts as a proton carrier and transports R718 through electro-osmotic drag, enabling compression under approximately isothermal conditions. This near-isothermal behavior arises because compression proceeds over a large electrochemically active surface area rather than through localized mechanical work, allowing the generated heat to be effectively dissipated. As a result, the pressure of the mixture increases with a limited temperature rise, which fundamentally differs from the isentropic compression characteristic of mechanical compressors. The compressed mixture then flows into the condenser and leaves the condenser at (state 3). At this stage, the flow is divided into two streams owing to phase separation. Because hydrogen behaves as a non-condensable gas under the operating conditions, only R718 is condensed in the condenser. As a result, the condensed liquid R718 stream exits the system at (state 4), while the remaining gas-phase stream consists of hydrogen with a small amount of R718 vapor. The condensed liquid R718 at (state 4) follows the refrigerant loop and passes through the expansion valve, undergoing isenthalpic expansion (state 5). The expanded R718 then flows through the evaporator, where it absorbs heat and evaporates, exiting the evaporator at (state 6). In parallel, the gas-phase stream separated at (state 3) follows a secondary flow path. This stream, composed primarily of hydrogen with residual R718 vapor, exits the phase separator at (state 7). Because hydrogen acts as a carrier gas rather than a refrigerant and does not participate in phase-change heat transfer, this stream bypasses the evaporator. The hydrogen-rich stream is expanded to the evaporator pressure at (state 8) to ensure pressure compatibility prior to recombination. Finally, the evaporator outlet stream (state 6) and the expanded hydrogen-rich stream (state 8) are recombined in the mixing chamber, forming the mixed stream at (state 9). This mixed stream is then supplied back to the system inlet (state 1), completing the thermodynamic cycle shown in Fig. 1(b).

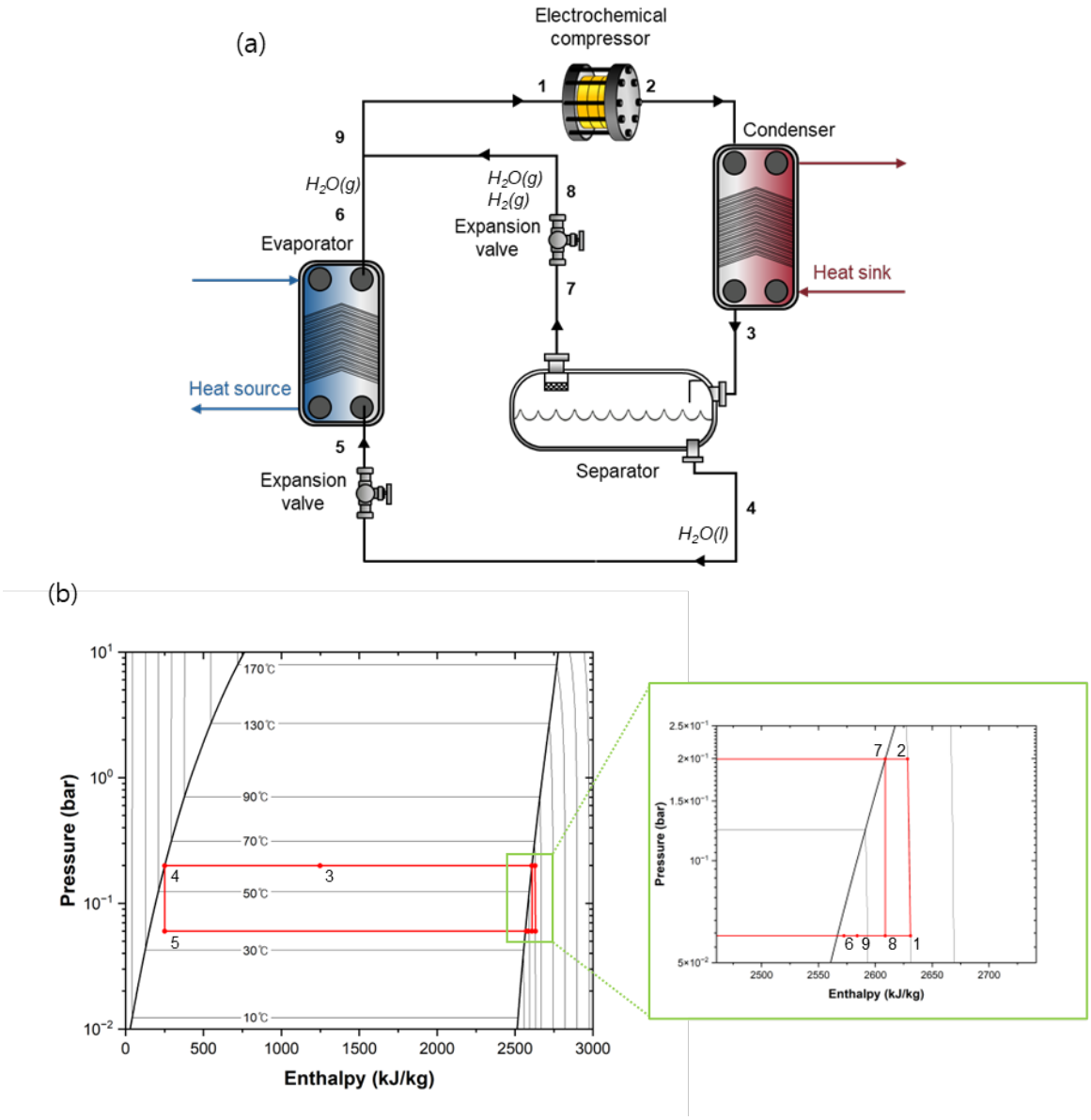

Figure 1. (a) Schematic of the proposed R718 heat pump systems using EC, (b) P-h diagram of R718 heat pump system using EC.

2.2. Modeling

To examine the operating characteristics of the R718 heat pump system using an EC, a system-level thermodynamic model was developed using MATLAB and REFPROP. The model describes the coupled behavior of electrochemical compression, phase change of R718, heat transfer in the heat exchangers, and separation and mixing of the R718/hydrogen mixture under steady-state conditions. The assumptions of this study are as follows:

- The compressor is assumed to operate under isothermal conditions because efficient heat removal maintains all components, including the membrane and bipolar plates, at a uniform target temperature.
- The electrical power consumption in this model represents the electrochemical energy required to sustain refrigerant transport through the membrane. Additional power associated with circulation or thermal management is not included, as the analysis focuses on the coupling between electrochemical transport and heat pump performance rather than on hardware-specific energy consumption.
- Given that temperature and pressure are not close to the critical value, a mixture of gases behaves ideally. The R718/H_2 gas used in heat pump system was considered an ideal gas.

2.2.1. Compression process in EC for R718

The power consumption of the EC is obtained below:

$$P_{stack} = n_{stcak}(E_{Nernst} + E_{ohmic} + E_{activation}) \times I \quad (1)$$

where n_{stcak} is the number of cell in the EC stack.

The E_{Nernst} is reversible voltage shown below:

$$E_{Nernst} = E_0 + \frac{RT}{nF} ln(\frac{P_{outlet,H_2}}{P_{inlet,H_2}}) \quad (2)$$

where E_0 is the standard electrode potential of hydrogen, n is the number of electrons involved in the electrochemical reaction.

The $E_{activation}$ is activation overpotential related to electrochemical reaction shown below:

$$E_{activation} = \frac{RT}{2a_{inlet}F} ln\frac{I}{j_o A} \quad (3)$$

where a_{inlet} is the transfer coefficient at inlet side, and j_0 is the exchange current density.

The E_{ohmic} is ohmic overpotential related to the mole flow rate of refrigerants through the membrane that is shown below:

$$\eta_{ohmic} = R_m I \quad (4)$$

where R_m is membrane resistance that is inversely proportional to conductivity of the membrane.

The mole flow rate of R718 through the compressor is obtained as follows.

The three terms in the right-hand side are mole flow rate of R718 by electro-osmotic drag, back diffusion, and pressure difference that are shown below:

$$\dot{n} = \dot{n}_{R718,EOD} - \dot{n}_{R718,bd} - \dot{n}_{R718,dp} \quad (5)$$

$$\dot{n}_{R718,EOD} = n_{drag}\frac{I}{F} \quad (6)$$

$$\dot{n}_{R718,bd} = -\frac{\rho_{dry}}{M_m} D_\lambda \frac{d\lambda}{dt} \quad (7)$$

$$\dot{n}_{R718,dp} = -c_{R718}\frac{k_p}{\mu}\frac{dP_{R718}}{dt} \quad (8)$$

where ρ_{dry} is the density of the dry membrane, M_m is the equivalent weight of the membrane, c_{R718} is the concentration of R718, k_p is the permeability of R718 through the membrane, and μ is the viscosity of R718. Here, n_{drag} is the electro-osmotic drag coefficient, which is the number of R718 molecules dragged by protons, λ is the content of R718 in the membrane, and D_λ is the diffusion coefficient of R718 across the membrane.

2.2.2. Thermodynamics properties of R718/hydrogen mixture in the heat pump system

The heat exchanger used in the model is assumed as plate type counter flow heat exchanger. We also assumed that the mixture of R718 and hydrogen is uniformly distributed, and no pressure drop in the heat exchanger. The overall heat transfer coefficient of the heat exchanger is shown below.

$$\frac{1}{U} = R_{total} = \frac{1}{h_{cool}} + \frac{1}{h_{ref}} + \frac{t_p}{k_p} \quad (9)$$

Here, U is overall heat transfer coefficient, h_{cool}, and h_{ref} are heat transfer coefficient and coolant and refrigerant mixture. The t_p is thickness of the heat exchanger plate, and k_p is conductive heat transfer coefficient of heat exchanger.

The heat transfer coefficient of coolant is obtained as below.

$$h_{cool} = \frac{Nu_{cool}}{D_h} k_{cool} \quad (10)$$

Here, D_h is hydraulic diameter, k_{cool} is thermal conductivity of coolant, and Nu_{cool} is Nusselt number of coolant shown below.

$$Nu_{cool} = 1.3204 Re^{0.5388} Pr^{0.4} (\frac{\mu}{\mu_w})^{0.14} \quad (11)$$

Here, Re is Reynolds number, Pr is Prandtl number, μ is dynamic viscosity, and μ_w is dynamic viscosity in the heat exchanger wall. The heat transfer coefficient of refrigerant mixture is obtained by follows.

$$Nu_{ref} = 1.18 Re^{0.374} x_{h2}^{-0.956} Ja^{-0.765} \quad (12)$$

Here, x_{h2} is mole fraction of hydrogen, and Ja is Jakob number that can show the ratio of sensible and latent heat shown below.

$$x_{h2} = \frac{P - P_{sat}}{P} \quad (13)$$

$$Ja = \frac{c_p(T - T_w)}{h_{fg}} \quad (14)$$

Here, c_p is specific heat of refrigerant mixture, T is the temperature of refrigerant mixture, h_{fg} is latent heat during phase change. T_w is the temperature of heat exchanger wall that is assumed as the same temperature of coolant because the thickness of the heat exchanger wall is thin.

The heat transfer in the heat exchanger is obtained below.

$$\dot{Q} = UA_t\Delta T_{lm} \tag{15}$$

$$\Delta T_{lm} = \frac{(T_{ref,in}-T_{cool,out})-(T_{ref,out}-T_{cool,in})}{ln\left(\frac{T_{ref,in}-T_{cool,out}}{T_{ref,out}-T_{cool,in}}\right)} \tag{16}$$

Here, A_t is area of heat exchanger, $T_{ref,in}$ and $T_{ref,out}$ are temperature of refrigerant at heat exchanger inlet and outlet, and $T_{cool,in}$ and $T_{cool,out}$ are temperature of coolant at inlet and outlet of the exchanger. The outlet temperatures of refrigerants and coolant are obtained by iterative method. Using the heat transfer in condenser and evaporator, we can obtain the enthalpy at the end of heat exchangers as shown below.

$$h_{cond,out} = h_{cond,in} - \frac{\dot{Q}_H}{\dot{m}_{ref}} \tag{17}$$

$$h_{eva,out} = h_{eva,in} + \frac{\dot{Q}_L}{\dot{m}_{R718,liq}} \tag{18}$$

Here, $h_{cond,out}$ and $h_{cond,in}$ are enthalpies at condenser outlet and inlet, respectively, and $h_{eva,out}$ and $h_{eva,in}$ are enthalpies at evaporator outlet and inlet, respectively. $\dot{m}_{ref}$ is mass flow rate of the R718/hydrogen mixture, and $\dot{Q}_H$ and $\dot{Q}_L$ are heat transfer at condenser and evaporator, respectively.

The heat transfer in the heat exchanger is obtained below.

$$\dot{Q} = UA_t\Delta T_{lm} \tag{19}$$

The COP of the heat pump system for R718/hydrogen mixture using EC is calculated below.

$$COP = \frac{\dot{Q}}{P_{stack}} \tag{20}$$

The parameters used in the modelling are listed in Table 1.

Table 1. Parameters for R718 heat pump using EC modeling.

Variables	Value	Unit
Thickness of membrane	0.009	cm
Density of dry membrane	1.9685×10^{-3}	$kg\cdot cm^{-3}$
Water permeability	2.002×10^{-19}	cm^2
Water viscosity	3.565×10^{-3}	$g\cdot cm^{-1}\cdot s^{-1}$
Active area	19.625	cm^2
Cell number	200	-
Exchange current density	0.470	$A\cdot cm^{-2}$
Plate thickness	7×10-4	m
Thermal conductivity of plate	17	$W\cdot m^{-1}\cdot K^{-1}$
Kinematic viscosity of the coolant	5.5×10-7	$m^2\cdot s^{-1}$
Prandtl number of the coolant	6.9	-
Specific heat of the coolant	4182	$J\cdot kg^{-1}\cdot K^{-1}$
Thermal conductivity of the coolant	0.6	$W\cdot m^{-1}\cdot K^{-1}$

2.3. Experimental Set-up

As shown in Fig.2, R718 is introduced into the EC by humidifying the hydrogen stream, forming an R718/hydrogen mixture for electrochemical compression. The hydrogen flow rate is accurately controlled using a mass flow controller. The temperature of the refrigerant mixture is regulated by a heating tape installed along the pipeline and continuously monitored with a digital temperature indicator. The mass flow rate of the R718/hydrogen mixture is governed by a programmable DC power supply, which applies either constant-voltage or constant-current operation to the electrochemical cell. Electrical power consumption is measured in real time using a digital power meter by simultaneously recording the applied voltage and current. After compression, the gas mixture passes through a plate-type heat exchanger, where heat is removed by a chiller, leading to partial condensation of R718. The resulting two-phase stream enters a phase separator, in which

liquid R718 is separated from the hydrogen gas. The hydrogen stream is released, while the condensed R718 is expanded through an expansion valve. The expanded R718 subsequently enters an evaporator, where it exchanges heat with a thermostatic bath and fully evaporates before discharge. Temperatures and pressures at key locations in the system are measured using T-type thermocouples and pressure transmitters, respectively. All measurement signals and control operations are performed using a LabVIEW-based data acquisition and control system. Each experimental condition is tested five times to ensure repeatability, and the reported results correspond to averaged values. A summary of the specifications and measurement uncertainties of the experimental equipment is provided in Table 2.

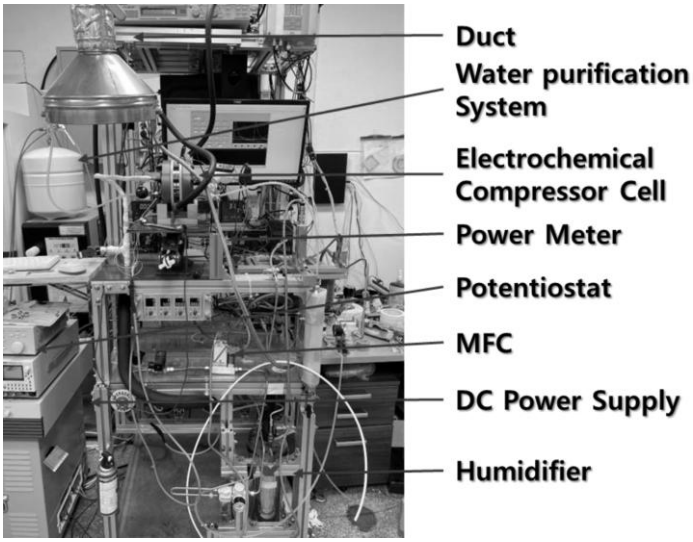

Figure 2. Experimental setup

Table 2. Specification of the devices used in this study.

Device	Purpose	Uncertainty
DC Power supply	Voltage and current supply	±0.1%
Power meter	Voltage and current measurements	±0.05%
Mass flow controller	Gas-flow control and measurement	±1%
Pressure transmitter	Pressure measurement	±0.25%
Indicator	Temperature control	±0.5%
Thermocouple	Temperature measurement	±0.75%
Chiller/heater	Coolant temperature control	±0.75℃

3. Results and discussion

This section presents a comprehensive performance evaluation of the proposed R718 heat pump system incorporating an EC. A system-level model was used to quantify the effect of condenser pressure, and evaporator pressure on cooling capacity, refrigerant distribution, and compressor power consumption.

3.1. Model validation

Before analyzing the system-level behavior, each major component of the model, including the EC, evaporator, and condenser, was validated against experimental results, as shown in Fig. 3. The EC model was validated by evaluating its power consumptnio over a range of mass flow rates and pressure ratios. The average modeling error was approximately 5.66%. The error increased with increasing mass flow rate across all pressure ratios, which is attributed to variations in local gas composition at high flow conditions. The power

consumption of the EC increased with both mass flow rate and pressure ratio. For example, at a mass flow rate of 1 g/min and a pressure ratio of 4, the power consumption reached 35 W. Because the mass flow rate is directly related to the applied current, higher flow rates require greater electrical power input. In addition, increasing the pressure ratio from 2 to 6 resulted in an 11.37% increase in power consumption at 1 g/min, primarily due to the increased reversible work associated with higher pressure differentials. The evaporator and condenser models were also validated using experimental data. The modeling errors were 12% for the evaporator and 18% for the condenser. The evaporator exhibited higher accuracy because heat transfer occurred with pure R718, whereas the condenser showed relatively lower accuracy owing to composition changes and the presence of non-condensable hydrogen during condensation. These levels of agreement confirm that the model captures the dominant thermodynamic behavior and can be reliably used for parametric analysis of the full system.

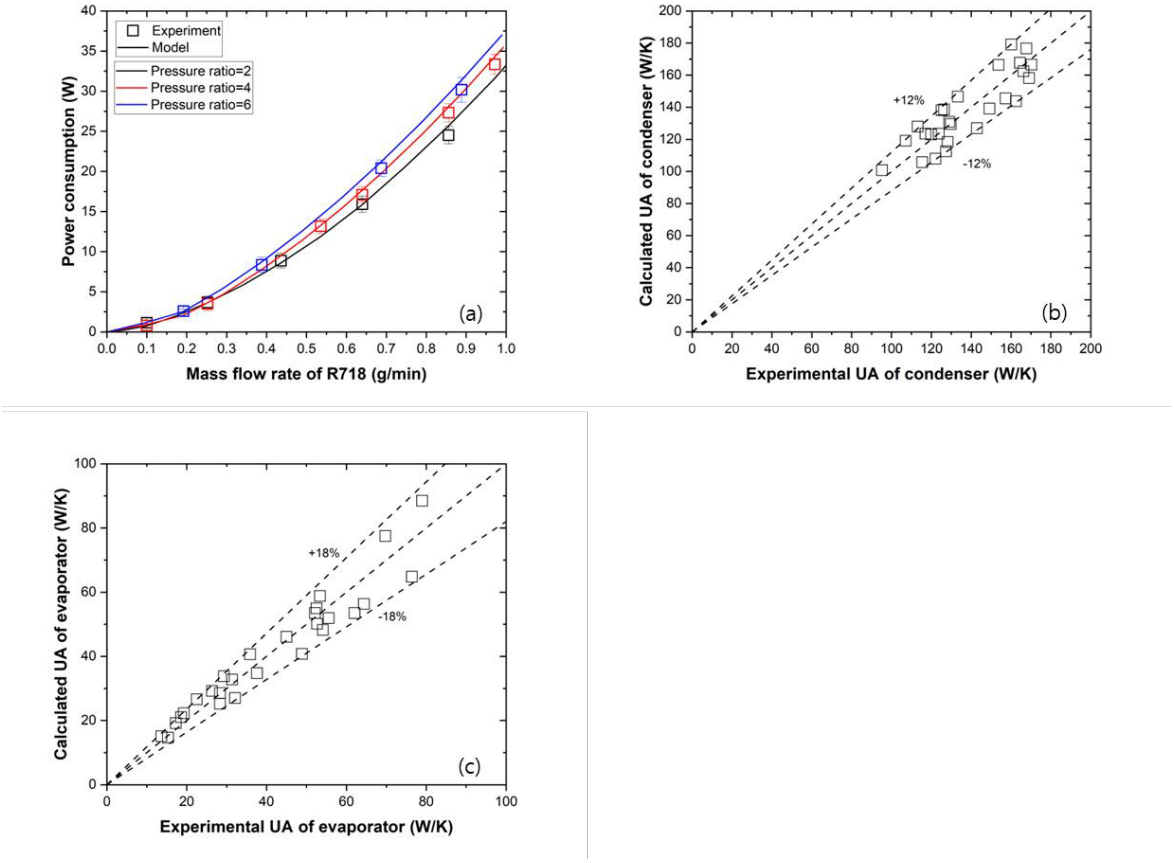

Figure 3. Model validation: (a) Validation of EC model for R718, (b) validation of evaporator that pure R718 flow, (c) validation of condenser that R718/hydrogen mixture flow

3.2. Effect of condenser pressure on system performance

Fig. 4 shows the variation of COP as a function of condenser pressure. The result was carried out at a low mass flow rate of 0.2 g/min, at which the modeling accuracy is less influenced by overpotential effects, membrane dehydration, and composition-dependent uncertainties that become pronounced at higher flow rates. The COP exhibits a non-monotonic dependence on condenser pressure, which can be explained by the coupled thermodynamic and electrochemical effects in the system. As the condenser pressure increases from 0.3 bar to 0.6 bar, the COP increases from approximately 3.1 to a maximum value of 4.2. This improvement is attributed to enhanced condensation of R718 at higher saturation temperatures, which increases the temperature difference between the refrigerant and the coolant in the condenser. The resulting improvement in condensation efficiency leads to a larger mass flow rate of liquid R718 supplied to the evaporator, thereby increasing the

cooling capacity through liquid–vapor phase change. When the condenser pressure exceeds 0.6 bar, the COP gradually decreases despite continued improvement in condensation. In this higher-pressure region, the increase in compressor power consumption becomes dominant. Because the condenser pressure is directly governed by the outlet pressure of the electrochemical compressor, further increases in pressure result in a nearly linear rise in electrical power input, while the incremental gain in cooling capacity diminishes. Consequently, the additional compression work outweighs the benefit of increased refrigerant flow, leading to a reduction in COP at elevated condenser pressures.

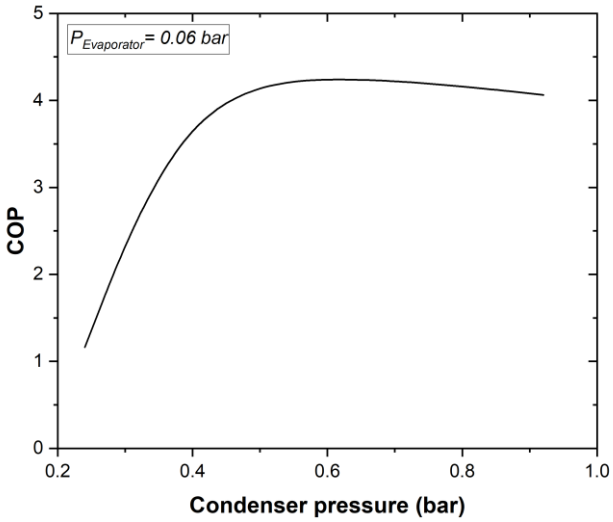

Figure 4. COP variations depending on condenser pressure.

However, the influence of condenser pressure extends beyond condensation. As more R718 transitions to the liquid phase at higher pressures, the vapor exiting the separator becomes increasingly hydrogen-rich. This shift in composition modifies the thermophysical properties of the circulating vapor mixture entering the EC. A higher hydrogen fraction lowers the partial pressure and mole fraction of R718 in the vapor phase, which affects membrane hydration, electro-osmotic drag behavior, and the overall transport resistance within the membrane. Although these effects do not immediately dominate system performance, they progressively reduce the contribution of R718 transport through drag-driven mechanisms and increase the reliance on pressure-driven transport, making the electrochemical compression process more sensitive to pressure ratio.

The most significant factor governing the eventual decline of COP at high condenser pressures is the rapid increase in the reversible electrochemical work required for compression. In an electrochemical compressor, the minimum electrical work is directly linked to the chemical potential difference between the inlet and outlet, which scales with the logarithmic ratio of their pressures. Therefore, any increase in condenser pressure proportionally raises the reversible voltage that must be supplied to maintain the same flow rate. Unlike mechanical compressors, where temperature rise partially offsets compression work, the EC operates under near-isothermal conditions, meaning that almost all of the required work must be provided electrically. As a result, the electrical power demand increases more rapidly than the cooling capacity once the condenser pressure exceeds a certain threshold.

Furthermore, the interplay between mixture composition and electrochemical transport intensifies this trend. A hydrogen-rich vapor mixture entering the EC reduces the effective drag coefficient and diminishes the coupling between proton transport and R718 movement. Consequently, a larger portion of the total transport must be achieved by overcoming the pressure difference across the membrane, which further elevates the electrical energy consumption. This compounding effect causes the power input to rise at a rate that eventually surpasses the thermal benefit gained from enhanced condensation.

Taken together, the evolution of COP with condenser pressure is governed by the balance between two competing phenomena: (1) increased condensation at higher saturation temperatures, which improves cooling capacity; and (2) elevated reversible and pressure-driven electrochemical work, which increases the electrical power required for compression. At low to moderate condenser pressures, the thermodynamic benefit of enhanced condensation outweighs the additional electrical work, leading to an increase in COP. At higher

pressures, however, the sharp rise in electrochemical work becomes dominant, resulting in a decline in COP. This leads to a clearly defined optimal condenser pressure at which the system achieves its highest efficiency.

3.3. Effect of evaporator pressure on system performance

The effect of evaporator pressure on COP is shown in Fig. 5. Based on the previous results, in which the COP was maximized at a condenser pressure of 0.6 bar, the compressor outlet pressure was fixed 0.6 bar for this analysis. As the evaporator pressure increased from 0.04 bar to 0,07 bar, the COP increased nearly linearly from 3.8 to 4.6. The influence of evaporator pressure on system performance differs fundamentally from that of condenser pressure, because variations in evaporator pressure do not significantly affect the condensation process or the phase distribution of the refrigerant mixture. Instead, its impact is primarily associated with changes in the compression ratio of the EC and the corresponding electrochemical work. As the evaporator pressure increases, the inlet pressure of the EC increases accordingly, which directly reduces the overall pressure ratio between the inlet and outlet. Because the reversible voltage of the EC scales with the logarithmic pressure ratio, even a moderate increase in evaporator pressure leads to a meaningful reduction in the minimum electrical work required to maintain the same molar flow rate. This reduction in electrochemical work is the primary reason for the observed improvement in COP at higher evaporator pressures.

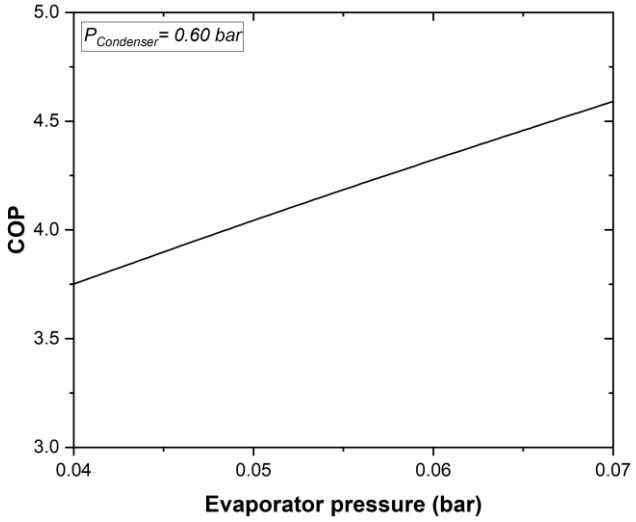

Figure 5. COP variations depending on evaporator pressure

Unlike the condenser-side behavior, changes in evaporator pressure do not substantially affect the saturation conditions or condensation efficiency of R718, meaning that the mass flow rate of condensed liquid reaching the evaporator remains essentially constant across the investigated pressure range. As a result, the cooling capacity is largely insensitive to evaporator pressure, and the system maintains nearly identical thermal output regardless of whether the evaporator operates at lower or higher pressure levels. This stability arises because the evaporator receives a fixed quantity of liquid R718 determined by upstream condensation, and the enthalpy change associated with evaporation is not significantly altered by the slight variations in inlet pressure and temperature observed in this system.

The composition of the vapor-phase refrigerant mixture returning to the EC also remains nearly unchanged with evaporator pressure. Since the condensation process is controlled predominantly by the condenser-side thermodynamic conditions, raising the evaporator pressure does not appreciably shift the vapor–liquid equilibrium or the amount of noncondensable hydrogen present in the vapor stream. Consequently, the hydrogen-to-R718 ratio entering the EC remains stable, preserving the membrane hydration state, the electro-osmotic drag coefficient, and the transport characteristics within the membrane. This constancy in mixture composition ensures that the EC's transport resistance and activation behavior remain unaffected by evaporator-side variations, reinforcing the dominance of pressure-ratio-driven reversible power in determining overall performance trends.

The improvement in COP with increasing evaporator pressure can therefore be attributed almost exclusively to the reduction in electrochemical power consumption. As the pressure ratio decreases, the reversible component of the EC voltage drops, and the total electrical power input decreases correspondingly. Because the cooling capacity remains nearly constant, any reduction in required electrical power translates directly into an improved COP. This relationship creates a monotonic increase in COP with increasing evaporator pressure, in contrast to the non-monotonic behavior observed on the condenser side. Importantly, the monotonic trend also indicates that, within the operating range evaluated in this study, the evaporator pressure does not approach a point where further increases would meaningfully degrade system performance through decreased refrigerant latent heat or reduced evaporation temperature lift. The evaporator remains fully effective in delivering the required thermal load, and the thermal balance within the heat exchanger is maintained. This suggests that, for the EC-driven R718 system, optimizing the evaporator pressure is primarily a matter of selecting a level that minimizes the compression ratio while maintaining practical limits such as refrigerant temperature, system safety, and component operational constraints.

4. Conclusion

This study investigated the performance of an R718 heat pump system driven by an electrochemical compressor. A validated system model was used to examine how condenser pressure and evaporator pressure influence cooling capacity, mixture behavior, and electrochemical compression work.

Through parametric analyses, a clear optimal operating condition with respect to condenser pressure was identified. The COP increased from approximately 3.1 at 0.3 bar to a maximum value of 4.2 at 0.6 bar, corresponding to an improvement of about 35%, while further increases in condenser pressure resulted in a decline in performance. This optimal point arises from the balance between enhanced condensation of R718, which improves cooling capacity, and the increased electrochemical work required for compression at higher pressure ratios. In addition, increasing evaporator pressure within the investigated range led to a monotonic improvement in COP by reducing the overall compression ratio and the associated electrochemical work.

These results demonstrate that the performance of R718 heat pump systems using electrochemical compression is strongly governed by the trade-off between thermodynamic phase-change benefits and electrochemical energy requirements. These findings indicate that electrochemical compression offers a viable pathway for overcoming the intrinsic limitations of R718 in conventional vapor-compression systems. Future work will extend the present framework by considering the effects of dynamic operating conditions, along with broader experimental validation across a wider range of mass flow rates, to enhance the understanding of electrochemical heat pump behavior under practical operating scenarios.

Acknowledgements

This work was supported by Korea Institute of Energy Technology Evaluation and Planning(KETEP) grant funded by the Korea government(MOTIE)(NO. 20212050100010, Chemisorption heat pump system using electrochemical compressor), the National Research Foundation of Korea(NRF) grant funded by the Korea government(MSIT) (No. 2022R1C1C1010338), National Institute of Standard and Technology, and the National Research Council of Science & Technology (NST) grant by the Korea government (MSIT) (CRC23041-000).

References

[1] Chu C, Kim M, Kim Y, Park S, Beom T, Kim S, et al. Serial electrochemical hydrogen compressor stack for high-pressure compression. Appl Energy 2025;383:125397. https://doi.org/10.1016/J.APENERGY.2025.125397.

[2] Chu CH, Kim YK, Kim MS, Kim S, Kim M, Kim DK. Effect of back diffusion on energy efficiency of electrochemical ammonia compressor. Int J Hydrogen Energy 2024;81:950–63. https://doi.org/10.1016/J.IJHYDENE.2024.07.351.

[3] Tao Y, Hwang Y, Radermacher R, Wang C. Experimental study on electrochemical compression of ammonia and carbon dioxide for vapor compression refrigeration system. International Journal of Refrigeration 2019;104:180–8. https://doi.org/10.1016/J.IJREFRIG.2019.05.009.

[4] Kim Y, Chu C, Beom T, Park S, Gu B, Kim S, et al. Feasibility study on electrochemical compressor utilizing water-hydrogen heat pump system. Energy Convers Manag 2025;334:119832. https://doi.org/10.1016/J.ENCONMAN.2025.119832.

[5] Kim YS, Kim DK, Ahn KY, Kim MS. Real-time analysis of dry start-up characteristics of polymer electrolyte membrane fuel cell with water storage process under pressurized condition. Energy 2020;199:117292. https://doi.org/10.1016/j.energy.2020.117292.

[6] Jafari A, Sadeghianjahromi A, Wang CC. Experimental and numerical investigation of brazed plate heat exchangers – A new approach. Appl Therm Eng 2022;200:117694. https://doi.org/10.1016/J.APPLTHERMALENG.2021.117694.

[7] Chouhan A, Aryal UR, Bahar B, Prasad AK. Analysis of an electrochemical compressor stack. Int J Hydrogen Energy 2020;45:31452–65. https://doi.org/10.1016/J.IJHYDENE.2020.08.164.